SIAM J. Appl. Math.
Vol. 75, No. 5, pp. 2050–2071

ASYMPTOTIC ANALYSIS OF A MAGNETIZED TARGET FUSION REACTOR*

MICHAEL LINDSTROM†

Abstract. Nonlinear conservation laws with moving boundaries often arise in applications such as gas dynamics and more recently in the context of nuclear fusion reactors. Gaining insight into the nature of solutions to such models and their dependence upon design parameters is often done numerically. We use formal asymptotics to study a model of a magnetized target fusion reactor for producing energy. We will asymptotically solve the compressible Euler equations with two free moving boundaries, with an algebraic coupling of fluid pressure at one of the free boundaries. The model consists of an intense pressure being imparted on the boundary of a large sphere holding molten lead-lithium over a very short time scale, in the middle of which is a smaller concentric sphere containing plasma. A localized disturbance quickly propagates toward the plasma, whereby part of the energy is reflected and part compresses the plasma. The plasma pressure is modeled by a magnetic pressure, dependent upon its radius. Both the outer boundary of the lead-lithium sphere and the plasma boundary are free. Using matched asymptotics and various techniques for solving linear hyperbolic systems including Riemann invariants and using the velocity potential formulation of the linear acoustic equations, we estimate the maximum compression of the plasma. This estimation gives insights into the factors relevant in designing an energy-producing reactor.

Key words. compressible Euler equations, hyperbolic conservation laws, free boundaries, formal asymptotics, magnetized target fusion

AMS subject classifications. 76L05, 41A60, 35L40, 35L45, 35L50, 35L65, 35L67, 35Q31, 35R37

DOI. 10.1137/140984142

1. Introduction.

Developing technology suitable for harvesting fusion energy and using it for power is an exciting and active area of research. Thanks to advances in technology, various projects worldwide have gotten closer to achieving this aim [4]. Building suitable technology is a long and expensive process and mathematical modeling has become an essential element to the designs. Recently, a paper was written illustrating a numerical framework that could be used in simulations of magnetized target fusion; in the paper, a simplified model of one particular reactor design was investigated [16]. In this paper, we investigate the model further from an analytic perspective.

This paper is organized into the following sections: this introduction, where we overview the physical motivation and context for the problem; section 2, where we outline the equations and nondimensionalize them; section 3, where we use formal asymptotic analysis to study the system; section 4, where we validate the asymptotics by comparing with numerical results; and finally section 5, where we conclude and consider future work. More details on the analysis and further exposition are provided in [15].

1.1. A design for a magnetized target fusion reactor.

Nuclear fusion is a complicated process whereby lighter elements fuse together to produce heavier ele-

*Received by the editors August 28, 2014; accepted for publication (in revised form) June 25, 2015; published electronically September 15, 2015. This work was funded in part by a scholarship from Westcoast Energy, Inc.
http://www.siam.org/journals/siap/75-5/98414.html
†Mathematics Department, University of California, Los Angeles, Box 951555, Los Angeles, CA 90095-1555 (mikel@math.ucla.edu).

ments. Fusion technology researchers often consider the use of deuterium or tritium fuels, producing helium and free neutrons upon fusion [1]. The released energy can be collected and used. Many factors impact fusion, but three very big factors in determining if a deuterium or tritium fuel can fuse to yield more energy output than input are pressure (or particle density), temperature, and confinement time [14]. In general, the greater the density and temperature that can be achieved and for the longer time, the more effective the device. The design we consider is based on a Canadian fusion research company, General Fusion [10], [11]. The apparatus being engineered consists of a large sphere of molten lead with a vertical axis that is empty through which a toroidal plasma will be fired. Pistons will impart a large pressure to the outer sphere over a fast time scale. This will generate a disturbance in the fluid which will propagate and focus radially inward, reaching the center. The plasma will be fired into the central axis at a precise time so as to be at the center when the pressure wave reaches it.

Our objective in this paper is to predict the minimal radius of the plasma, as this is a key parameter in how efficient such a design could potentially be. The parameter regime for the device winds up being at the boundary of asymptotic validity; we will furnish a minimum radius that is qualitatively consistent with the numerics in its parameter sensitivity, but where the quantitative accuracy is a loose estimate. Our work also validates that the asymptotics are quantitatively accurate given a well-ordered parameter regime. Other factors besides the minimum radius, such as confinement time, are not analyzed here.

1.2. Physical assumptions. We take the plasma to be spherical and we assume spherical symmetry for all components. Plasma pressures have both a gas pressure and a magnetic pressure component. In many plasmas, the magnetic pressure is much larger initially. We model the plasma pressure by a magnetic pressure (scaling inversely with the fourth power of its radius) [21], neglecting the gas pressure component. Our motivation for this is not to say the gas pressure will always be negligible, but rather to gain more detailed qualitative information about the most basic of the system parameters.

The pressure imparted by the pistons is described by a baseline pressure plus a very large pressure modulated by a Gaussian with a very short time scale. The pressure of lead-lithium is taken to be linear in density. Our model will neglect mixing effects and radiation losses. These simplifications allow us to write more tractable equations and gain qualitative insight into how the most basic engineering parameters influence the compression of the plasma.

2. Equations and nondimensionalization. Here we present the equations relevant to this study and nondimensionalize the system so that formal asymptotics can be applied. The values and explanations of the constants used are provided in Tables 1 and 2. A dimensionless diagram of our model is given in Figure 1.

2.1. Euler equations. Within the lead-lithium, we work with the Euler equations for mass and momentum conservation. With radial symmetry, in a space-time coordinate system (R, T) we have

$$\varrho_T + (\varrho V)_R + \frac{2}{R}(\varrho V) = 0 \quad \text{and} \quad (\varrho V)_T + P_R + (\varrho V^2)_R + \frac{2}{R}(\varrho V^2) = 0, \tag{2.1}$$

where ϱ is the mass density, V is the radial velocity, and P is the pressure.

From experimental data, the sound speed C_s and density ϱ_0 of lead at atmospheric pressure P_{atm} are known [19]. The square of the sound speed is the derivative of P

TABLE 1
Characteristic constants for this application.

Variable	Description	Value
C_s	Sound speed of lead at 1 atm	2090 m/s
ϱ_0	Density of lead at 1 atm	11,340 kg/m^3
P_{atm}	Atmospheric pressure	101,325 Pa
$P_{\text{plasma},0}$	Initial plasma pressure	5 MPa
$P_{\max}$	Maximum piston pressure	2 GPa
Γ	Coefficient for magnetic pressure growth	8000 N m^2
T_0	Guassian decay time scale	45 μs
$R_{\text{inner},0}$	Initial plasma radius	0.2 m
$R_{\text{outer},0}$	Initial lead sphere radius	1.5 m

TABLE 2
Characteristic dimensions for the system. The first three entries are chosen by the theoretical operating conditions. The last two entires can be derived from the first three.

Variable	Notation/Equation	Characteristic scale
Density ϱ	$\bar{\varrho} = \varrho_0$	$11,340$ kg m^{-3}
Pressure P	$\bar{P} = P_{\max}$	2 GPa
Distance R	$\bar{R} = R_{\text{outer},0}$	1.5 m
Time T	$\bar{T} = \bar{R}\sqrt{\bar{\varrho}/\bar{P}}$	3.57 ms
Velocity V	$\bar{V} = \sqrt{\bar{P}/\bar{\varrho}}$	420. m s^{-1}

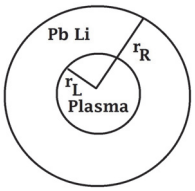

FIG. 1. *The geometry we consider is spherically symmetric with r_L and r_R free boundaries.*

with respect to density ϱ [20] allowing us to express $P(\rho)$ as an approximate linear function:

$$P(\varrho) = C_s^2(\varrho - \varrho_0) + P_{\text{atm}}. \tag{2.2}$$

We approximate the equation of state of lead-lithium by the linearized equation of state for lead and permit negative absolute pressures. Negative absolute pressures are observed over short time scales in some materials [7].

2.2. Initial conditions. The maximum piston pressure occurs at $T = 0$, but we allow for negative times relative to this. The system begins at $T = -\infty$, where

$$V(R,-\infty) = 0, \quad P(R,-\infty) = \frac{\Gamma}{R_L(-\infty)^4}, \quad \varrho(R,-\infty) = \frac{P(R,-\infty) - P_{\text{plasma},0}}{C_s^2} + \varrho_0 \tag{2.3}$$

with

$$R_L(-\infty) = R_{\text{inner},0} \quad \text{and} \quad R_R(-\infty) = R_{\text{outer},0}. \tag{2.4}$$

2.3. Boundary conditions. Due to the impact of the pistons and the interaction of the wave with the plasma boundary, this is a moving boundary problem. We denote R_L to be the radius of the inner wall of the lead-lithium sphere (the plasma radius) and R_R to be the radius of the outer wall of the lead-lithium sphere. The local fluid velocity at the inner and outer boundaries matches the velocities of these walls, respectively:

$$V_L(T) \equiv \frac{\mathrm{d}R_L}{\mathrm{d}T} = V(R_L(T), T) \quad \text{and} \quad V_R(T) \equiv \frac{\mathrm{d}R_R}{\mathrm{d}T} = V(R_R(T), T). \tag{2.5}$$

At any given time, the lead-lithium exists between R_L and R_R.

At the inner wall, the pressure is given by the plasma magnetic pressure. This gives

$$P_L(T) = P(R_L(T), T) = \frac{\Gamma}{R_L(T)^4} = \frac{P_{\text{plasma},0}}{(R_L(T)/R_L(-\infty))^4}, \tag{2.6}$$

where Γ is a constant chosen so that with $P_L = \Gamma R_L^{-4}$, $P_L(R_L(-\infty)) = P_{\text{plasma},0}$. This is an algebraic coupling of the fluid pressure and plasma pressure at this wall. At the outer wall, the pressure is given by the piston pressure which is modeled by a Gaussian pressure in addition to a baseline minimum applied pressure

$$P_R(T) = (P_{\max} - P_{\text{plasma},0})e^{-T^2/T_0^2} + P_{\text{plasma},0}. \tag{2.7}$$

2.4. Nondimensionalization. To nondimensionalize, we will look at (2.1) with the change of variables $\varrho = \bar{\varrho}\rho$, $V = \bar{V}v$, $P = \bar{P}p$, $R = \bar{R}r$, $T = \bar{T}t$, where the bars denote characteristic dimensional quantities and ρ, v, p, r, and t are dimensionless. We wind up with

$$\frac{\bar{\varrho}}{\bar{T}}\rho_t + \frac{\bar{\varrho}\bar{V}}{\bar{R}}(\rho v)_r + \frac{\bar{\varrho}\bar{V}}{\bar{R}}\frac{2}{r}(\rho v) = 0 \quad \text{and} \quad \frac{\bar{\varrho}\bar{V}}{\bar{T}}(\rho v)_t + \frac{\bar{P}}{\bar{R}}p_r + \frac{\bar{\varrho}\bar{V}^2}{\bar{R}}(\rho v^2)_r + \frac{\bar{\varrho}\bar{V}^2}{\bar{R}}\frac{2}{r}(\rho v^2) = 0. \tag{2.8}$$

By matching dimensional terms in $(2.8)_1$ and $(2.8)_2$, we have

$$\bar{V} = \bar{R}/\bar{T}, \tag{2.9}$$

$$\bar{\varrho} = (\bar{P}\bar{T})/(\bar{R}\bar{V}). \tag{2.10}$$

Equations (2.9) and (2.10) give good guidance as to reasonable scalings for the system, and we also have some freedom. We will choose $\bar{R} = 1.5$ m, the initial outer radius; $\bar{\varrho} = 11340$ kg/m^3, the density of lead at atmospheric pressure; and $\bar{P} = 2$ GPa, the maximum pressure imparted on the outer wall. Table 2 summarizes these results.

2.5. Selecting an asymptotic parameter. Through the nondimensionalization, various dimensionless parameters appear. Upon considering the physics of the problem, an intense pressure imparted over a very short time scale (45μs $\ll 3.57$ ms), we will define $\epsilon = T_0/\bar{T} = 0.0126$ such that the Gaussian component of the pressure becomes $\mathrm{e}^{-(t\bar{T}/T_0)^2} = \mathrm{e}^{-t^2/\epsilon^2}$. With respect to this value of ϵ, the different dimensionless parameters have characteristic orders. For example, in dimensionless form, $p = c^2(\rho - 1) + d$, where $c^2 = C_s^2\bar{\varrho}/\bar{P} \approx 24.7$ and $d = P_{\text{atm}}/\bar{P} \approx 5.07 \times 10^{-5}$. The density of lead-lithium corresponding to the maximum pressure is 1.04, which is well described by $\rho = 1 + O(\epsilon)$. If $\rho = 1 + O(\epsilon)$ corresponds to $p = O(1)$, then $c^2 = O(\epsilon^{-1})$.

TABLE 3
Dimensionless parameters of the system.

Variable	Meaning	Formula	Value
ϵ	pulse time scale	$\frac{T_0}{\bar{R}\sqrt{\bar{\varrho}/\bar{P}}}$	0.0126
b	scaled sound speed	$\frac{C_s\sqrt{\epsilon}}{\sqrt{\bar{P}/\bar{\varrho}}}$	0.557
γ	scaled magnetic pressure coefficient	$\frac{P_{\text{plasma},0}R_{\text{inner},0}^4}{\bar{P}\bar{R}^4\epsilon^{7/2}}$	3.52
χ	scaled initial inner radius	$\frac{R_{\text{inner},0}}{\bar{R}\sqrt{\epsilon}}$	1.19

Thus, it is reasonable to write $p(\rho) = \frac{b^2}{\epsilon}(\rho-1)+a\epsilon^{5/2}$, where $b = 0.557$ and $a = 2.84$. In fact, since we are aiming for a leading order behavior of the system, we will neglect $a\epsilon^{5/2}$ entirely. Also due to its negligible size, $O(\epsilon^{3/2})$, we neglect the dimensionless $P_{\text{plasma},0}$ term in the pressure condition at the right wall. Discarding these terms can be justified a posteriori by noting that in all the analysis to come, only pressures that are $O(\epsilon)$ balance in the relevant equations.

Proceeding in a similar way with the remaining equations and boundary conditions, and making use of the fact that knowing either p or ρ is equivalent, the final set of equations and conditions we consider are presented below, valid for $r_L < r < r_R$, $-\infty < t < \infty$. In due course, all these equations will be used.

$$\rho_t + (\rho v)_r + \frac{2}{r}(\rho v) = 0, \quad (\rho v)_t + \frac{b^2}{\epsilon}\rho_r + (\rho v^2)_r + \frac{2}{r}(\rho v^2) = 0, \tag{2.11}$$

$$p = \frac{b^2}{\epsilon}(\rho - 1), \tag{2.12}$$

$$v_L(t) = \frac{\mathrm{d}r_L}{\mathrm{d}t} = v(r_L(t),t), \quad v_R(t) = \frac{\mathrm{d}r_R}{\mathrm{d}t} = v(r_R(t),t), \tag{2.13}$$

$$p_L(t) = p(r_L(t),t) = \frac{\gamma\epsilon^{7/2}}{r_L(t)^4}, \quad p_R(t) = p(r_R(t),t) = \mathrm{e}^{-t^2/\epsilon^2}, \tag{2.14}$$

$$v(r,-\infty) = 0, \quad p(r,-\infty) = \frac{\gamma\epsilon^{7/2}}{r_L(-\infty)^4}, \quad \rho(r,-\infty) = 1, \tag{2.15}$$

$$r_L(-\infty) = \chi\epsilon^{1/2}, \quad r_R(-\infty) = 1. \tag{2.16}$$

We summarize the constants in Table 3. Our main objective is to estimate the smallest value of r_L which we denote r^*.

3. Formal asymptotic analysis. The analysis has five distinct phases: I, formation; II, focusing; III, reflecting; IV, slow collapse; and V, maximum compression. See Figure 2. Effectively I is an inner region that is matched to II; III is an inner region that can match to II and which matches to IV over a long time; and V is an inner region to IV.

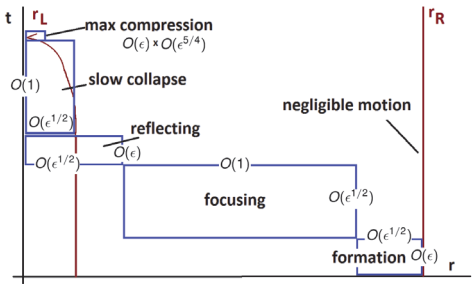

FIG. 2. *Relevant space-time scales and boundary motion. In phase* I*, pulses are formed, moving toward the plasma. In phase* II*, the pulses move radially inward, growing in amplitude due to focusing. In phase* III*, the pulses interact with the plasma with much of the energy reflecting but a small portion of useful energy remaining. In phase* IV*, the plasma slowly begins to collapse, and in phase* V*, the maximum compression is reached.*

3.1. Phase I.

3.1.1. Pulse formation setup. To analyze the formation of the pulse, we scale with the following independent and dependent variables: $t = \epsilon\tau$, $y = \frac{r-1}{\epsilon}$, $\rho \sim 1 + \epsilon\rho_1 + \epsilon^{3/2}\rho_2$, and $v \sim \epsilon^{1/2}v_0 + \epsilon v_1$.

This gives

$$\rho_{1,\tau} + v_{0,y} = 0, \quad v_{0,\tau} + b^2\rho_{1,y} = 0, \tag{3.1}$$

$$\rho_{2,\tau} + v_{1,y} = -2v_0, \quad v_{1,\tau} + b^2\rho_{2,y} = 0. \tag{3.2}$$

To deal with boundary conditions, we find $r_R \sim 1 + \epsilon^{3/2}r_{R0}(\tau)$. It is worth mentioning that when we write $r_{R0}(\tau)$ we really mean $r_{R0}(t = \epsilon\tau)$ and not $r_{R0}(t = \tau)$! Throughout this paper we use the shorthand that a dependent variable evaluated at a rescaled variable should be interpreted by the proper scalings in the original (r, t) variables.

The outer wall changes by a distance $O(\epsilon^{3/2})$. If we denote y_R as the position of the outer boundary in the y-coordinates, then $y_R = \frac{r_R-1}{\epsilon^{1/2}} = \epsilon r_{R0}(\tau) + \cdots$. The boundary condition that must be upheld is $p_R(\tau) = \frac{b^2}{\epsilon}(\rho - 1) = \mathrm{e}^{-\tau^2}$ so that

$$\rho_1(r_R(\tau), \tau) + \epsilon^{1/2}\rho_2(r_R(\tau), \tau) = \frac{1}{b^2}\mathrm{e}^{-\tau^2}.$$

We can now perform a Taylor expansion (since the problem is linear and the forcing terms are continuous and differentiable). Keeping just a few terms, we obtain $b^2(\rho_1(0, \tau) + \rho_{1y}(0, \tau)(\epsilon r_{R0}) + \epsilon^{1/2}\rho_2(0, \tau)) = \mathrm{e}^{-\tau^2}$, which implies

$$\rho_1(0, \tau) = \frac{1}{b^2}e^{-\tau^2} \quad \text{and} \quad \rho_2(0, \tau) = 0. \tag{3.3}$$

As far as initial conditions go,

$$\rho_1(y, -\infty) = \rho_2(y, -\infty) = v_0(y, -\infty) = v_1(y, -\infty) = 0. \tag{3.4}$$

3.1.2. Riemann invariants. Both the leading order and first correction terms can be written in the form

$$\begin{pmatrix} \rho_\tau \\ v_\tau \end{pmatrix} + \begin{pmatrix} 0 & 1 \\ b^2 & 0 \end{pmatrix} \begin{pmatrix} \rho_y \\ v_y \end{pmatrix} = \begin{pmatrix} f(y, \tau) \\ g(y, \tau) \end{pmatrix} \tag{3.5}$$

and such problems can be solved effectively with a technique known as Riemann invariants [3].

Observe the 2×2 matrix has eigenvalues $\pm b$ with corresponding left eigenvectors $\ell^{\pm} = (\pm b, 1)$. Upon left multiplying (3.5) by $\ell^{\pm}$, we obtain $(\pm b\rho + v)_\tau \pm b(\pm b\rho + v)_y = \pm bf + g$. Thus, the system has characteristics. Denoting $c^{\pm} = \pm b\rho + v$, we have that along $\mathrm{d}y/\mathrm{d}\tau = \pm b$, $\mathrm{d}c^{\pm}/\mathrm{d}\tau = \pm f + g \equiv h^{\pm}$. Given that $\rho = v = 0$ at $\tau = -\infty$, (so $c^{\pm} = 0$ at $\tau = -\infty$) we can compute $c^{+}(y,\tau) = 0 + \int_{-\infty}^{\tau} h(\tilde{y}(\tilde{\tau}), \tilde{\tau})\mathrm{d}\tilde{\tau}$, where $\tilde{y}(\tilde{\tau}) = y + b(\tilde{\tau} - \tau)$ describes the straight pathway along the rightgoing characteristic starting at $\tau = -\infty$ and reaching (y, τ). Thus,

$$c^{+}(y,\tau) = \int_{-\infty}^{\tau} h^{+}(y + b(\tilde{\tau} - \tau), \tilde{\tau})\mathrm{d}\tilde{\tau}.$$

To find $c^{-}(y,\tau)$, we need to know its value at the point along the τ-axis whose leftgoing characteristics eventually reach (y,τ). As c^{+} is known along the τ-axis, and ρ is also specified there, we can find c^{-}. The leftgoing characteristic path leading to (y,τ) can be described by $(\tilde{y}(\tilde{\tau}), \tilde{\tau}) = (b(\tau - \tilde{\tau}) + y, \tilde{\tau})$ for $\tau + y/b \le \tilde{\tau} \le \tau$. From $c^{+}(0, \tau + y/b) = b\rho(0, \tau + y/b) + v(0, \tau + y/b)$ we get $c^{-}(0, \tau + y/b) = -b\rho(0, \tau + y/b) + v(0, \tau + y/b) = c^{+}(0, \tau + y/b) - 2b\rho(0, \tau + y/b)$. We thus have

$$c^{-}(y,\tau) = c^{+}(0, \tau + y/b) - 2b\rho(0, \tau + y/b) + \int_{\tau + y/b}^{\tau} h^{-}(b(\tau - \tilde{\tau}), \tilde{\tau})\mathrm{d}\tilde{\tau}.$$

Given $c^{\pm}$, we can recover

$$\rho = \frac{1}{2b}(c^{+} - c^{-}) \quad \text{and} \quad v = \frac{1}{2}(c^{+} + c^{-}).$$

3.1.3. Phase I results. Using the Riemann invariants to solve (3.2), (3.3), and (3.4), in the distinguished limit, we have

$$\rho \sim 1 + \epsilon \frac{1}{b^2} e^{-(\tau + y/b)^2} - \epsilon^{3/2} \frac{y}{b^2} e^{-(\tau + y/b)^2} \tag{3.6}$$

and

$$v \sim \epsilon^{1/2} \frac{-1}{b} e^{-(\tau + y/b)^2} + \epsilon \left(\frac{\sqrt{\pi}}{2} \mathrm{erfc}(-\tau - y/b) + \frac{y}{b} e^{-(\tau + y/b)^2} \right). \tag{3.7}$$

A plot of these solutions at $\tau = 1$ is given in Figure 3. In the r-coordinates, the characteristic widths of these pulses are $O(\sqrt{\epsilon})$. The plot includes numerical validation of the results, which are discussed in more detail in section 4.

To leading order, the density and velocity are described by leftgoing plane waves. Due to the scalings, we have been looking on such a small scale that the system hasn't quite "noticed" the spherical nature of the problem and everything appears flat (for $y = O(1)$). The divergent terms with y prefactors, however, actually result from the spherical geometry, as we shall see in the following section.

3.2. Phases II and III.

3.2.1. Spherical focusing setup. Having obtained the basic shape of the pulses being formed, we can now analyze how these pulses behave as they move toward the center of the sphere. From phase I, we have $\rho \sim 1 + \epsilon\rho_1 + \epsilon^{3/2}\rho_2$ and

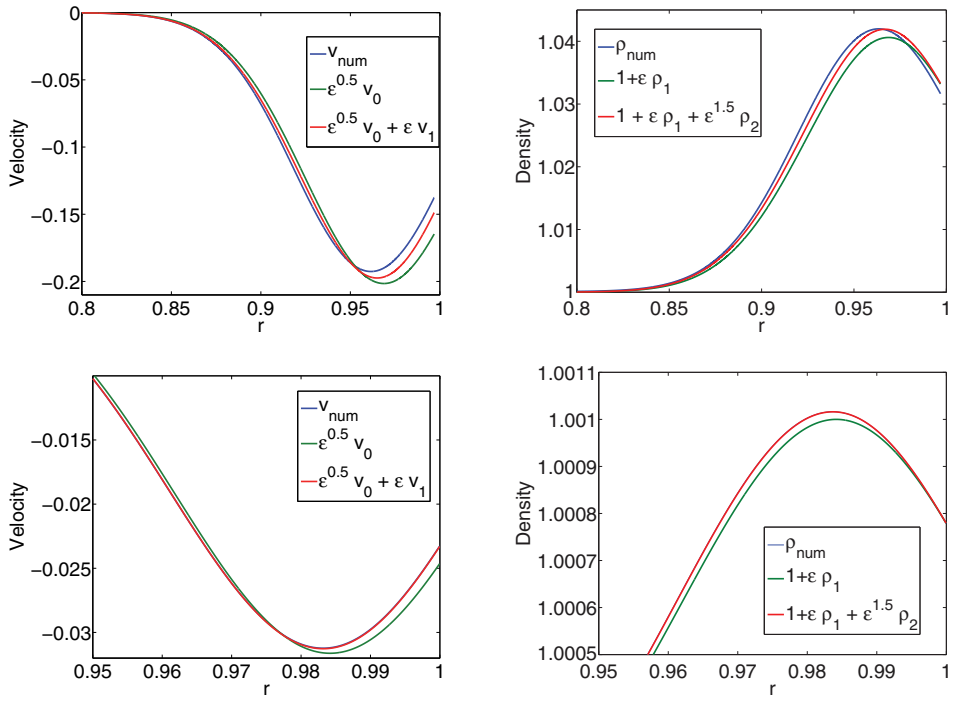

FIG. 3. *Plots depicting the profiles of the velocity and density at a very small value of t to validate the asymptotics of phase* I. *In the case of the second row, the two term asymptotic expansions agree so well with the numerics the plots cannot be distinguished. Parameters:* $b = 0.557, \chi = 1.19, \gamma = 3.52, \epsilon = 0.0126, t = \epsilon/2$ *(top row);* $b = \chi = \gamma = 1, \epsilon = 0.001, t = \epsilon/2$ *(bottom row).*

$v \sim \epsilon^{1/2} v_0 + \epsilon v_1$ and we shall make a similar ansatz here. We will consider $r = O(1)$ and choose a time scale $t = \epsilon^{1/2} T$ to obtain the equations

$$\rho_{1,T} + v_{0,r} + \frac{2}{r} v_0 = 0 \quad \text{and} \quad v_{0,T} + b^2 \rho_{1,r} = 0,$$

where the identical equations are upheld for ρ_2 and v_1.

The initial and boundary conditions are more subtle here. They cannot be written down clearly because of the different time scales (typically, to match at $T = 0$, we would require $\tau \to \infty$, but in this case, the solutions found in phase I tend to 0). However, by solving the hyperbolic systems at different orders, we can find the functional form of the solution, which allows us to find the solutions by matched asymptotics.

3.2.2. Spherical linear acoustic limit. For the two leading orders, the systems of PDEs that need to be solved are of the form

$$\rho_T + v_r + \frac{2}{r} v = f \quad \text{and} \quad v_T + b^2 \rho_r = g. \tag{3.8}$$

Such equations also appear in linear acoustic problems, often with $f = g = 0$ (and in our case we will not need to explicitly solve such an equation with $f, g \neq 0$).

To solve this, we will make use of a velocity potential $\phi(r, T) = \int_\infty^r v(s, T) \mathrm{d}s$. With this substitution, we have

$$\rho_T + \phi_{rr} + \frac{2}{r} \phi_r = f \quad \text{and} \quad \phi_{rT} + b^2 \rho_r = g. \tag{3.9}$$

Integrating $(3.9)_2$ from $r=\infty$, assuming $\rho=0$ at $r=\infty$, we have $\phi_T(r,T)+b^2\rho(r,T)=\int_\infty^r g(s,T)\mathrm{d}s\equiv G(r,T)$ so that $\phi_{TT}=-b^2\rho_T+G_T$. Using $(3.9)_1$ here now gives $\phi_{TT}=-b^2(-\phi_{rr}-\frac{2}{r}\phi_r+f)+G_T$ so

$$\phi_{TT}=b^2\left(\phi_{rr}+\frac{2}{r}\phi_r\right)+G_T-b^2f. \tag{3.10}$$

Note that by taking a time derivative of $(3.8)_1$ and a space derivative of $(3.8)_2$ we have

$$\rho_{TT}=-v_{rT}-\frac{2}{r}v_T+f_T \quad \text{and} \quad v_{rT}=g_r-b^2\rho_{rr}. \tag{3.11}$$

Equations $(3.11)_2$ and $(3.11)_1$ can then be used in $(3.8)_1$ to obtain $\rho_{TT}=-(g_r-b^2\rho_{rr})-\frac{2}{r}(g-b^2\rho_r)+f_T$ so that

$$\rho_{TT}=b^2\left(\rho_{rr}+\frac{2}{r}\rho_r\right)+f_T-\frac{2}{r}g-g_r. \tag{3.12}$$

A symmetry argument now helps to solve (3.10) and (3.12). If $\phi=\Phi/r$ and $\rho=K/r$, then $\phi_{rr}+\frac{2}{r}\phi_r=\frac{\Phi_{rr}}{r}$, and similarly for K. Thus we can transform these equations into one-dimensional wave equations [20]:

$$\Phi_{TT}=b^2\Phi_{rr}+S_1(r,T), \quad K_{TT}=b^2K_{rr}+S_2(r,T) \tag{3.13}$$

with $S_1(r,T)=r(G_T-b^2f)$, and $S_2(r,T)=r(f_T-\frac{2}{r}g-g_r)$.

3.2.3. Leading order and correction in outer region. The system of equations for ρ_1 and v_0 and ρ_2 and v_1 are the same, and in both cases the source terms are fortunately zero. With no source terms, and with only leftgoing waves (since there are no sources going right), the solutions of (3.13) are $K=P(r+bT)$ and $\Phi=Q(r+bT)$, respectively. Then, being mindful of the fact that the pulses generated have a width of size $O(\sqrt{\epsilon})$ and are leftgoing originating near $r=1$, we can write the solutions to the systems of equations as $\rho_1=\frac{1}{r}P_1(\frac{r-1+bT}{\sqrt{\epsilon}})$, $\rho_2=\frac{1}{r}P_2(\frac{r-1+bT}{\sqrt{\epsilon}})$, $v_0=\frac{1}{r}Q_0'(\frac{r-1+bT}{\sqrt{\epsilon}})-\frac{\sqrt{\epsilon}}{r^2}Q_0(\frac{r-1+bT}{\sqrt{\epsilon}})$, and $v_1=\frac{1}{r}Q_1'(\frac{r-1+bT}{\sqrt{\epsilon}})-\frac{\sqrt{\epsilon}}{r^2}Q_1(\frac{r-1+bT}{\sqrt{\epsilon}})$.

By taking these solutions, expressing them in the inner (y,τ)-coordinates, and applying the Van Dyke matching of inner and outer solutions [8], our distinguished limit is that

$$\rho\sim 1+\epsilon\left(\frac{1}{b^2r}\mathrm{e}^{-(\frac{r-1+bT}{b\sqrt{\epsilon}})^2}\right)+o(\epsilon^{3/2}) \tag{3.14}$$

and

$$v\sim\epsilon^{1/2}\left(\frac{-1}{br}\mathrm{e}^{-(\frac{r-1+bT}{b\sqrt{\epsilon}})^2}\right)+\epsilon\left(\frac{\sqrt{\pi}}{2r^2}\mathrm{erfc}\left(-\frac{r-1+bT}{b\sqrt{\epsilon}}\right)\right)+o(\epsilon). \tag{3.15}$$

3.2.4. Leading order and correction in inner region. As the pulses move inward, due to the $1/r$ and $1/r^2$ terms, the amplitudes grow and the asymptotic expansions we arrived at above lose their validity. To describe the region where the pulses have grown and arrive at the inner wall, we rescale space and time. We let $r=\epsilon^{1/2}\sigma$ and $t-t_s=\epsilon\hat{t}$, where t_s is a shifting parameter such that the peak of the leftgoing pressure wave will have reached the plasma wall at $r=\chi\epsilon^{1/2}$ at $\hat{t}=0$.

We anticipate different scalings for the asymptotic expansions. From $r = O(1)$ to $r = O(\sqrt{\epsilon})$, the first perturbation term in the density perturbation given in (3.14) should have grown from $O(\epsilon)$ to $O(\sqrt{\epsilon})$. Similarly, from (3.15), the velocity amplitude should have grown from $O(\sqrt{\epsilon})$ to $O(1)$ and the velocity term that was $O(\epsilon)$ should also become $O(1)$ since it grows like $1/r^2$. Therefore, in this next inner region, we write $\rho \sim 1 + \epsilon^{1/2}\rho_1 + \epsilon\rho_2$ and $v \sim v_0 + \epsilon^{1/2}v_1$. Using $\partial_r = \epsilon^{-1/2}\partial_\sigma$ and $\partial_t = \epsilon^{-1}\partial_{\hat{t}}$, (2.11) becomes

$$\rho_{1,\hat{t}} + v_{0,\sigma} + \frac{2}{\sigma}v_0 = 0, \quad v_{0,\hat{t}} + b^2\rho_{1,\sigma} = 0 \tag{3.16}$$

and

$$\rho_{2,\hat{t}} + v_{1,\sigma} + \frac{2}{\sigma}v_1 = -(\rho_1 v_0)_\sigma - \frac{2}{\sigma}\rho_1 v_0, \quad v_{1,\hat{t}} + b^2\rho_{2,\sigma} = -(\rho_1 v_0)_{\hat{t}} - (v_0^2)_\sigma - \frac{2}{\sigma}v_0^2. \tag{3.17}$$

By virtue of the fact that these PDEs can be solved and matched to the outer solution (as done in the following paragraphs), we can be confident in the scalings chosen. We will now consider boundary conditions. For a time scale that is $O(\epsilon)$, given a velocity $v = O(1)$, the inner wall can only move a distance $O(\epsilon)$ and thus the inner wall position remains $O(\sqrt{\epsilon})$ (recall that $r_L(-\infty) = \chi\sqrt{\epsilon}$). We can find the leading order nonzero contribution to the inner wall motion in the $(\sigma, \hat{t})$-coordinates. We define $\sigma_L = r_L/\sqrt{\epsilon}$. Then $\sigma_L(\hat{t}) = \chi + \int_{-\infty}^{\hat{t}} \sqrt{\epsilon}v(\sigma_L(\hat{s}), \hat{s})\mathrm{d}\hat{s}$. The factor of $\sqrt{\epsilon}$ comes from the fact that $\frac{\mathrm{d}r_L}{\mathrm{d}t} = v(r_L(t), t) = \frac{\mathrm{d}\epsilon^{1/2}\sigma_L}{\mathrm{d}\epsilon\hat{t}} = \epsilon^{-1/2}\frac{\mathrm{d}\sigma_L}{\mathrm{d}\hat{t}}$. Thus,

$$\sigma_L(\hat{t}) = \chi + \int_{-\infty}^{\hat{t}} \sqrt{\epsilon}v(\chi + O(\sqrt{\epsilon}), \hat{s})\mathrm{d}\hat{s} = \chi + \epsilon^{1/2}\int_{-\infty}^{\hat{t}} v(\chi, \hat{s})\mathrm{d}\hat{s} + O(\epsilon).$$

As the pressure at the inner wall is given by $p = \gamma\epsilon^{7/2}/r_L^4$, for $r_L = O(\sqrt{\epsilon})$, $p = O(\epsilon^{3/2}) = \frac{b^2}{\epsilon}(\epsilon^{1/2}\rho_1(\sigma_L, \hat{t}) + \epsilon\rho_2(\sigma_L, \hat{t}) + \cdots)$ so that by a Taylor expansion, $\epsilon^{1/2}\rho_1(\chi, \hat{t}) + \epsilon(\rho_{1\sigma}(\chi, \hat{t})\int_{-\infty}^{\hat{t}} v_0(\chi, \hat{s})\mathrm{d}\hat{s} + \rho_2(\chi, \hat{t})) + o(\epsilon) = 0$. This gives us boundary conditions

$$\rho_1(\chi, \hat{t}) = 0 \quad \text{and} \quad \rho_2(\chi, \hat{t}) = -\rho_{1\sigma}(\chi, \hat{t})\int_{-\infty}^{\hat{t}} v_0(\chi, \hat{s})\mathrm{d}\hat{s}. \tag{3.18}$$

If we again consider (3.16) in potential form with $\phi_0(\sigma, \hat{t}) = \int_\infty^\sigma v_0(\hat{\sigma}, \hat{t})\mathrm{d}\hat{\sigma}$, then by integrating the equation from $\sigma = \infty$ to $\sigma = \chi$, $\phi_{0\hat{t}}(\chi, \hat{t}) + b^2\rho_1(\chi, \hat{t}) = 0$, where we used $\rho_1 = \phi_0 = 0$ at $\sigma = \infty$. Since $\rho_1(\chi, \hat{t}) = 0$, we must have

$$\phi_{0\hat{t}}(\chi, \hat{t}) = 0. \tag{3.19}$$

Similarly by integrating (3.17) we have $\phi_{1\hat{t}}(\chi, \hat{t}) + b^2\rho_2(\chi, \hat{t}) = \int_{-\infty}^{\chi}(-(\rho_1 v_0)_{\hat{t}} - (v_0^2)_\sigma - \frac{2}{\sigma}v_0^2)\mathrm{d}\sigma$, which with $(3.18)_2$ gives

$$\phi_{1\hat{t}}(\chi, \hat{t}) = b^2\rho_{1\sigma}(\chi, \hat{t})\int_{-\infty}^{\hat{t}} v_0(\chi, \hat{s})\mathrm{d}\hat{s} + \int_{-\infty}^{\chi}\left(-(\rho_1 v_0)_{\hat{t}} - (v_0^2)_\sigma - \frac{2}{\sigma}v_0^2\right)\mathrm{d}\sigma. \tag{3.20}$$

We can find the form of the solution to (3.16) using the solutions of (3.13) with $S_1 = S_2 = 0$. We note that there are both incoming signals (from $\sigma = \infty$) and outgoing signals (from the interaction of the pulses with the plasma) so we have

waves propagating in both directions. Also, we are on a spatial scale of $O(\sqrt{\epsilon})$ so that it is not necessary to rescale the argument of the solutions like we did in the previous section. As $\hat{t} \to -\infty$, we will neglect the rightgoing wave and consider only the incoming wave. We write $\rho_1 = \frac{P_1^+(\sigma+b\hat{t})}{\sigma}$, $v_0 = \frac{Q_0^{+\prime}(\sigma+b\hat{t})}{\sigma} - \frac{Q_0^+(\sigma+b\hat{t})}{\sigma^2}$.

Expressing the outer solutions in (r,T)-coordinates in the inner coordinates and going to leading order, we have

$$\rho_1 = \frac{1}{b^2\sigma}\mathrm{e}^{-(\frac{\sigma-\chi}{b}+\hat{t})^2} \quad (\hat{t} \to -\infty) \tag{3.21}$$

and

$$v_0 = \frac{-1}{b\sigma}\mathrm{e}^{-(\frac{\sigma-\chi}{b}+\hat{t})^2} + \frac{\sqrt{\pi}}{2\sigma^2}\mathrm{erfc}\left(-\left(\frac{\sigma-\chi}{b}+\hat{t}\right)\right) \quad (\hat{t} \to -\infty).$$

These solutions are valid only for $\hat{t} \to -\infty$. To get solutions for other times, we first find the potential as $\phi_0 = \int_\infty^\sigma v_0(\sigma,\hat{t})\mathrm{d}\sigma$ so that $\phi_0 = -\frac{\sqrt{\pi}}{2\sigma}\mathrm{erfc}(-\frac{\sigma-\chi}{b} - \hat{t})$ $(\hat{t} \to -\infty)$. From $(3.18)_1$, in order for ρ_1 to be 0 along $\sigma = \chi$ and to have the incoming solution given in (3.21), the solution is

$$\rho_1 = \frac{1}{b^2\sigma}(\mathrm{e}^{-(\frac{\sigma-\chi}{b}+\hat{t})^2} - \mathrm{e}^{-(\frac{\chi-\sigma}{b}+\hat{t})^2}). \tag{3.22}$$

For the potential, we note that $\phi_0(\chi,-\infty) = -\frac{\sqrt{\pi}}{2\chi}\mathrm{erfc}(\infty) = 0$ so that by (3.19), $\phi_0(\chi,\hat{t}) = 0$ is the boundary condition for all $\hat{t}$. Using this, and the wave solution to ϕ_0, we must have that

$$\phi_0 = \frac{\sqrt{\pi}}{\sigma}\left(\mathrm{erfc}\left(-\frac{\chi-\sigma}{b} - \hat{t}\right) - \mathrm{erfc}\left(-\frac{\sigma-\chi}{b} - \hat{t}\right)\right)$$

so

$$v_0 = \frac{\sqrt{\pi}}{2\sigma^2}\left(\mathrm{erf}\left(\frac{\sigma-\chi}{b} - \hat{t}\right) - \mathrm{erf}\left(-\frac{\chi-\sigma}{b} - \hat{t}\right)\right) - \frac{1}{b\sigma}(\mathrm{e}^{-(\frac{\sigma-\chi}{b}+\hat{t})^2} + \mathrm{e}^{-(\frac{\chi-\sigma}{b}+\hat{t})^2}). \tag{3.23}$$

In writing the above equation, we used the fact that $\mathrm{erfc}(-x-y) - \mathrm{erfc}(x-y) = (1-\mathrm{erf}(-x-y)) - (1-\mathrm{erf}(x-y)) = \mathrm{erf}(x-y) - \mathrm{erf}(-x-y)$.

We note that the leading order density perturbation and velocity profiles grow in amplitude like $1/r$, or close to such scaling, at their peak values as the profiles move radially inward. This is consistent with known results for fluid dynamics with spherical symmetry [12]. Given the equation of state (2.12), this also means the peak pressure grows like $1/r$. To be more precise, the asymptotic profile for ρ_1 and p do grow like $1/r$, but because v_0 in the inner region also includes an error function term that reduces the magnitude of the Gaussian peak, the scaling may be slightly smaller. A typical profile of the velocity and pressure, computed numerically [16], is depicted in Figure 4. We also observe that v_0 and ρ_1 tend to 0 as $\hat{t} \to \infty$ and the total distance the plasma wall moves due to these leading order terms is $O(1) \times O(\epsilon) = O(\epsilon)$. More precisely the leading order displacement solely due to the v_0 term is

$$\delta_0 = \epsilon\int_{-\infty}^{\infty} v_0(\chi,\hat{t})\mathrm{d}\hat{t} = \epsilon\int_{-\infty}^{\infty}\frac{-2}{b\chi}\mathrm{e}^{-\hat{t}^2}\mathrm{d}\hat{t} = -\frac{2\sqrt{\pi}\epsilon}{b\chi}. \tag{3.24}$$

Any nonnegligible compression will be a result of the correction terms. Equations (3.17), $(3.18)_2$, and (3.20) give insights into what the effects of these correction terms are, which we discuss in the following portion of this paper.

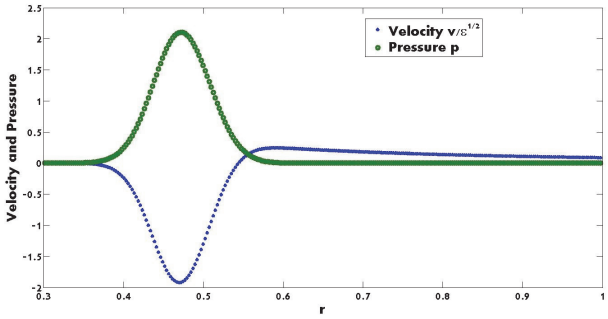

FIG. 4. *The pulses are moving to the left. The pressure peak grows like* $1/r$ *as the pulses move inwards. The velocity has a peak with negative value and one with positive value. The negative value grows roughly like* $1/r$. *Parameters:* $b = \chi = \gamma = 1$, $\epsilon = 0.0025$, $t = 0.0262$.

3.2.5. Phase III: Resultant velocity field. Given that most of the localized disturbances are reflected, the driving force for compression, if a substantial compression is to occur, must come from a residual negative radial velocity of the inner wall after the waves come in. We begin by considering the systems given by (3.17) in a time-independent regime (a long time after the v_0 and ρ_1 pulses have interacted with the inner wall). We then find that $v_{1\sigma} + \frac{2}{\sigma}v_1 = 0$ and $\rho_{2\sigma} = 0$ so that $v_1 = A/\sigma^2$ and $\rho_2 = B$. Physically, $\rho_2(\sigma = \infty) = 0$ so that $B = 0$, but the constant A cannot be determined. We can, however determine $\phi_1 = \int_{\infty}^{\sigma} \frac{A}{\hat{\sigma}^2} \mathrm{d}\hat{\sigma} = -A/\sigma(\hat{t} \to \infty)$. This suggests that the correction term leaves a velocity field behind that may do further work to compress the plasma. Stricly speaking, we show that the value of ϕ_1 approaches a constant at $\sigma = \chi$ as $\hat{t} \to \infty$ but section 4.3 validates this residual velocity field numerically.

Observe that $-\chi\phi_1(\chi, \infty) = A$ and $\phi_1(\chi, \infty) = \phi_1(\chi, -\infty) + \int_{-\infty}^{\infty} \phi_{1\hat{t}}(\chi, \hat{t})\mathrm{d}\hat{t}$.

At $\hat{t} = -\infty$, $v_1 = 0$, and $\phi_1(\chi, -\infty) = 0$. Then by using (3.20), we have

$$\begin{aligned}\phi(\chi, \infty) &= \int_{-\infty}^{\infty} \left[b^2 \rho_{1\sigma}(\chi, \hat{t}) \int_{-\infty}^{\hat{t}} v_0(\chi, \hat{s})\mathrm{d}\hat{s} + \int_{-\infty}^{\chi} \left(-(\rho_1 v_0)_{\hat{t}} - (v_0^2)_\sigma - \frac{2}{\sigma} v_0^2 \right) \mathrm{d}\sigma \right] \mathrm{d}\hat{t} \\ &= \int_{-\infty}^{\infty} \int_{\chi}^{\infty} \frac{2}{\sigma} v_0^2 \mathrm{d}\sigma \mathrm{d}\hat{t} > 0\end{aligned}$$

after evaluating the integrals and canceling terms. Thus, $A < 0$ and there is a remaining velocity field in the negative radial direction that can compress the plasma. Obtaining a simple expression for the exact value of this integral is not possible, but by taking note of the characteristic shape of the integrand, we can approximate it with high precision. We remark that

(3.25)

$$\begin{aligned} v_0^2 &= \left[\frac{\sqrt{\pi}}{2\sigma^2} \left(\mathrm{erf}\left(\frac{\sigma - \chi}{b} - \hat{t} \right) - \mathrm{erf}\left(-\frac{\chi - \sigma}{b} - \hat{t} \right) \right) - \frac{1}{b\sigma} (\mathrm{e}^{-(\frac{\sigma-\chi}{b} + \hat{t})^2} + \mathrm{e}^{-(\frac{\chi-\sigma}{b} + \hat{t})^2}) \right]^2 \\ &\approx \frac{1}{b^2\sigma^2} (\mathrm{e}^{-(\frac{\sigma-\chi}{b} + \hat{t})^2} + \mathrm{e}^{-(\frac{\chi-\sigma}{b} + \hat{t})^2})^2 \\ &\approx \frac{1}{b^2\sigma^2} (\mathrm{e}^{-2(\frac{\sigma-\chi}{b} + \hat{t})^2} + \mathrm{e}^{-2(\frac{\chi-\sigma}{b} + \hat{t})^2}) \\ &\approx \frac{1}{b^2\sigma^2} \frac{\sqrt{\pi}}{\sqrt{2}} \left(\delta\left(\hat{t} - \frac{\sigma - \chi}{b} \right) + \delta\left(\hat{t} - \frac{\chi - \sigma}{b} \right) \right), \end{aligned}$$

TABLE 4

Verifying the numerical validity of the approximation given in (3.25) *by doubling/halving the governing parameters and computing I^* with the approximation of v_0^2 given in* (3.25) *and the numerically integrated value.*

(b, χ)	I^*_{approx}	$I^*_{\text{numerical}}$
$(0.557, 1.19)$	5.75	5.71
$(1.11, 1.19)$	1.45	1.43
$(0.288, 1.19)$	22.5	22.8
$(0.557, 2.38)$	1.40	1.43
$(0.557, 0.595)$	23.5	23.8

where δ denotes the Dirac delta function [5]. We justify the first approximation by noting the terms with erf are modulated by a $1/\sigma^2$ which decays to 0 faster as $\sigma \to \infty$ than terms with $1/\sigma$ and that for $\sigma \approx \chi$, the two error functions are being subtracted and have similar arguments. The second approximation comes from the fact that a Gaussian is dominated by its behavior near its maximum and there is little overlap between the two Gaussians. The final approximation comes from approximating each Gaussian by its area modulating a delta function centered at its maximum.

From the approximation in (3.25),

$$\phi_1(\chi, \infty) = I^* \approx \int_{-\infty}^{\infty} \int_{\chi}^{\infty} \frac{2}{\sigma} \frac{1}{b^2\sigma^2} \frac{\sqrt{\pi}}{\sqrt{2}} \left(\delta\left(\hat{t} - \frac{\sigma - \chi}{b} \right) + \delta\left(\hat{t} - \frac{\chi - \sigma}{b} \right) \right) \mathrm{d}\sigma \mathrm{d}\hat{t} = \frac{\sqrt{2\pi}}{b^2\chi^2}.$$

Therefore $A \approx \frac{\sqrt{2\pi}}{b^2\chi}$. For the remainder of this paper, we will take this approximations as the value of I^*. Table 4 computes the integral $\int_{-\infty}^{\infty} \int_{\chi}^{\infty} \frac{2}{\sigma} v_0^2 \mathrm{d}\sigma \mathrm{d}\hat{t}$ using (3.25) and numerically, and the results show good agreement. With this A, the long-time velocity profile is

$$v \sim \sqrt{\epsilon} v_1 = \sqrt{\epsilon} \frac{-\sqrt{2\pi}}{b^2 \chi \sigma^2}. \tag{3.26}$$

3.2.6. Phase III results. After the pulses have interacted with the inner wall, there remains a residual velocity field which remains as a time-independent solution of the asymptotic equations. We find that $\rho \sim 1 + o(\epsilon)$ and $v \sim \frac{-\sqrt{2\pi}}{b^2\chi\sigma^2} \epsilon^{1/2} + o(\epsilon^{1/2})$.

3.3. Phases IV and V.

3.3.1. An energy argument. At this point we now compute the remaining kinetic energy (all the particles with a negative radial velocity), assuming there are no reflections at the right boundary and that all the useful energy is in the vicinity of the inner wall. Based on a kinetic energy density of $\mathcal{E} = \frac{1}{2}\rho v^2$, the total kinetic energy is

$$E = \frac{4\pi^2 \epsilon^{5/2}}{b^4 \chi^3}. \tag{3.27}$$

By equating this with the work done in compressing the plasma from $r_L = \chi\sqrt{\epsilon}$ to $r_L = r^*$,

$$W = 4\pi\gamma\epsilon^{7/2} \left(\frac{1}{r^*} - \frac{\epsilon^{-1/2}}{\chi} \right), \tag{3.28}$$

in the distinguished limit, the minimum radius is

$$r^* \sim \frac{b^4\chi^3\gamma}{\pi}\epsilon. \tag{3.29}$$

This sort of energy argument was originally used by Lord Rayleigh in considering the compression of a bubble in an incompressible fluid [17]. We present a formal asymptotic argument for this result in the next two subsections.

3.3.2. Outer region for motion of plasma boundary. To proceed with formal asymptotics, we need to consider higher orders of the equations of mass and momentum conservation. By taking the equations of (2.11) to two higher orders than presented in (3.17) with $\rho \sim 1+\epsilon^{1/2}\rho_1+\epsilon\rho_2+\epsilon^{3/2}\rho_3+\epsilon^2\rho_4$ and $v \sim v_0+\epsilon^{1/2}v_1+\epsilon v_2+\epsilon^{3/2}v_3$ we obtain the following balances:

$$\rho_{3,\hat{t}} + v_{2,\sigma} + \frac{2}{\sigma}v_2 = -(\rho_2 v_0 + \rho_1 v_1)_\sigma - \frac{2}{\sigma}(\rho_2 v_0 + \rho_1 v_1), \tag{3.30}$$

$$v_{2,\hat{t}} + b^2\rho_{3,\sigma} = -(\rho_1 v_0^2 + 2v_0 v_1)_\sigma - \frac{2}{\sigma}(\rho_1 v_0^2 + 2v_0 v_1) - (\rho_2 v_0 + \rho_1 v_1)_{\hat{t}}, \tag{3.31}$$

$$\rho_{4,\hat{t}} + v_{3,\sigma} + \frac{2}{\sigma}v_3 = -(\rho_3 v_0 + \rho_2 v_1 + \rho_1 v_2)_\sigma - \frac{2}{\sigma}(\rho_3 v_0 + \rho_2 v_1 + \rho_1 v_2), \tag{3.32}$$

$$\begin{aligned} v_{3,\hat{t}} + b^2\rho_{4,\sigma} &= -(\rho_2 v_0^2 + 2\rho_1 v_0 v_1 + 2v_0 v_2 + v_1^2)_\sigma - \frac{2}{\sigma}(\rho_2 v_0^2 + 2\rho_1 v_0 v_1 + 2v_0 v_2 + v_1^2) \\ &\quad - (\rho_3 v_0 + \rho_2 v_1 + \rho_1 v_2)_{\hat{t}}. \end{aligned} \tag{3.33}$$

From our previous considerations of the behavior of the solutions as $\hat{t} \to \infty$, we observe that (3.30) and (3.31) can also reach a steady solution with $\rho_3 = 0$ and $v_2 = \text{constant}/\sigma^2$ since ρ_1, ρ_2, v_0 all tend to 0, which eliminates all forcing terms in the equations. Looking at (3.32) and (3.33) similarly, we actually have residual forcing terms that do not vanish as $\hat{t} \to \infty$, namely, the terms with v_1^2. After a long time, we infer that $\rho \sim 1 + \epsilon^2\rho_4$ and $v \sim \epsilon^{1/2}v_1 + \cdots$. By scaling so that $t = \varpi$, an $O(1)$ time scale, we obtain a new PDE system to evolve, which serves as an outer region for a problem describing the motion of the plasma radius. Our balance is

$$v_{1,\sigma} + \frac{2}{\sigma}v_1 = 0, \quad v_{1,\varpi} + b^2\rho_{4,\sigma} + v_{1_\sigma}^2 + \frac{2}{\sigma}v_1^2 = 0. \tag{3.34}$$

Equation $(3.34)_1$ gives an effective incompressibility to the lead-lithium and we can proceed to solve (3.34) as done to derive the Rayleigh–Plesset equation for bubble dynamics [2]. From $(3.34)_1$ we have $v_1 = f(\varpi)/\sigma^2$ so that upon substituting this into (3.34) we have $\frac{f'}{\sigma^2} + b^2\rho_{4_\sigma} - \frac{2f^2}{\sigma^5} = 0$, which can be integrated from $\sigma = \infty$ to $\sigma = \sigma_L(\varpi)$ the position of the plasma inner radius in the σ-coordinates to get $\frac{-f'}{\sigma_L} + b^2\rho_4(\sigma_L) + \frac{f^2}{2\sigma_L^4} = 0$, where we used $\rho_4(\infty, \varpi) = 0$. We have $\rho_4(\sigma_L, \varpi) = 0$ as well because if $r = O(\sqrt{\epsilon})$, $p = O(\epsilon^{3/2})$ so that the density at the left boundary is $1 + O(\epsilon^{5/2})$. We then get

$$\frac{\mathrm{d}f}{\mathrm{d}\varpi} = \frac{f^2}{2\sigma_L^3}. \tag{3.35}$$

Additionally, the velocity at the inner wall $\frac{\mathrm{d}\sigma_L}{\mathrm{d}\varpi} = v_1(\sigma_L, \varrho)$ (due to the scaling in this regime there is no extra factor of $\sqrt{\epsilon}$ to deal with) so

$$\frac{\mathrm{d}\sigma_L}{\mathrm{d}\varpi} = \frac{f}{\sigma_L^2}. \tag{3.36}$$

Dividing (3.35) and (3.36) we find that $\frac{\mathrm{d}f}{\mathrm{d}\sigma_L} = \frac{f}{2\sigma_L}$, which has solution $f = C\sqrt{\sigma_L}$ for a constant C. Thus we can treat v_1 as a function of the inner wall position where $v_1(\sigma_L) = C/\sigma_L^{3/2}$ after using the solution in conjunction with (3.36). Given

$$v_1(\chi) = -\frac{\sqrt{2\pi}}{b^2\chi^3} \tag{3.37}$$

from (3.26), we have $C = \frac{-\sqrt{2\pi}}{b^2\chi^{3/2}}$ and with respect to these outer coordinates

$$v_1(\sigma_L) = \frac{-\sqrt{2\pi}}{b^2\chi^{3/2}\sigma_L^{3/2}}. \tag{3.38}$$

At this point, the system has not felt the effects of the plasma pressure and the wall is slowly accelerating inward.

3.3.3. Inner region for motion of plasma boundary. Numerous balances are possible for the system of (2.11) and it is possible to arrive at the scaling we choose here considering all possible balances and solutions and choose the one that can match to the outer region, but we will consider a physical argument here to obtain the balance. We seek a balance of terms where the pressure of the plasma resists the compression (i.e., the pressure gradient balances the momentum flux). We consider $r = O(\epsilon^c)$. If $r = O(\epsilon^c)$, then $p = O(\epsilon^{7/2-4c})$ and $\rho = 1 + O(\epsilon^{9/2-4c})$. Based on the growth predicted by (3.38) this would give a scaling of $v = O(\frac{\epsilon^{1/2}}{(\epsilon^c/\epsilon^{1/2})^{3/2}}) = O(\epsilon^{5/4-3c/2})$. The form of the scaling as written comes from the velocity growing like $1/r_L^{3/2}$ but being $O(\sqrt{\epsilon})$ when $r = O(\sqrt{\epsilon})$. To balance the pressure/density ρ term in the momentum equation with the v^2 terms, we require $7/2 - 4c = 5/2 - 3c$ so that $c = 1$. Now we let $r = \epsilon^1 z$. Then $v \sim \epsilon^{-1/4} v_{-1}$, $\rho \sim 1 + \epsilon^{1/2}\rho_1$, and to balance the scales of velocity times time equals distance, we pick $t = \epsilon^{5/4}\hat{\varpi}$, where $\hat{\varpi}$ measures a time with respect to an arbitrary reference point. The resulting balance is given by

$$v_{-1,z} + \frac{2}{z}v_{-1} = 0 \quad \text{and} \quad v_{-1,\hat{\varpi}} + b^2\rho_{1,z} + (v_{-1}^2)_z + \frac{2}{z}v_{-1} = 0. \tag{3.39}$$

Using the functional form of v_{-1} implied by $(3.39)_1$, $v_{-1} = g(\hat{\varpi})/z_L^2$, in $(3.39)_2$ and integrating as before, this time up to z_L, the position of the wall in the inner coordinates gives us $\frac{-g'}{z_L} + \frac{\gamma}{z_L^4} + \frac{g^2}{2z_L^4} = 0$, where we used $b^2\rho_1(z_L, \hat{\varpi}) = \gamma/z_L^4$. It follows then that $\frac{\mathrm{d}g}{\mathrm{d}\hat{\varpi}} = \frac{\gamma + g^2/2}{z_L^3}$ and $\frac{\mathrm{d}z_L}{\mathrm{d}\hat{\varpi}} = \frac{g}{z_L^2}$ yielding

$$v_{-1} = \frac{-\sqrt{2Dz_L - 2\gamma}}{z_L^2}. \tag{3.40}$$

Observe that when $z_L = z_L^* = \gamma/D$ the velocity is 0 to leading order and this will be our leading order estimate to the compression. To find D, we need to peform matched asymptotics between the inner and outer regions with respect to the functional dependence of the wall velocity upon the wall position.

3.3.4. Matching to determine minimum radius. We now put the outer variables of (3.38) in inner variables to match the behaviors as $z_L \to \infty$ and $\sigma_L \downarrow 0$,

$$\epsilon^{-1/4}(v_{-1})_{\text{inner}} = \epsilon^{1/2}(v_1)_{\text{outer}},$$
$$\epsilon^{-1/4}\frac{-\sqrt{2D}}{z_L^{3/2}} = \epsilon^{1/2}\frac{-\sqrt{2\pi}}{b^2\chi^{3/2}(\epsilon^{1/2}z_L)^{3/2}},$$

yielding $\frac{-\sqrt{2D}}{z_L^{3/2}} = \frac{-\sqrt{2\pi}}{b^2\chi^{3/2}z_L^{3/2}}$ so that $D = \frac{\pi}{b^4\chi^3}$. In the z variable, we have a minimum radius of $z_L^* = \gamma/D = \frac{b^4\chi^3\gamma}{\pi}$ and we thus find $r^* = \frac{b^4\chi^3\gamma}{\pi}\epsilon$ consistent with (3.29) found with the energy argument. While the energy argument was assumed true for incompressible fluids, it seems in the asymptotic limit compressibility does not influence the compression to leading order. Note that by having quarter powers of ϵ, it may become difficult to distinguish different asymptotic terms without taking ϵ to be extremely small. When $v = O(\epsilon^{-1/4})$, which is very close to the sound speed magnitude, the wave-like behavior of the equations may be close to breaking down. Indeed, when ϵ is too large, the local velocity magnitude can even exceed the sound speed during the compression phase.

3.3.5. Dimensional expression for plasma compression. We can finally go back to the dimensional parameters in our problem. Using Tables 2 and 3, we find the minimum radius is

$$R_L^* \approx \frac{C_s^4 P_{\text{plasma},0} R_{\text{inner},0}^7 \varrho_0^3}{\pi P_{\max}^4 R_{\text{outer},0}^4 T_0^2}, \tag{3.41}$$

where

$$\frac{T_0}{R_{\text{outer},0}}\frac{P_{\max}^{1/2}}{\varrho_0^{1/2}} \ll 1, \quad \frac{C_s T_0^{1/4} P_{\max}^{1/4}}{R_{\text{outer},0}^{1/2}\varrho_0^{1/4}} = O(1), \quad \frac{P_{\text{plasma},0}R_{\text{inner},0}^4\varrho_0^{7/4}}{P_{\max}^{11/4}R_{\text{outer},0}^{1/2}T_0^{7/4}} = O(1),$$
$$\frac{R_{\text{inner},0}\varrho_0^{1/4}}{R_{\text{outer},0}^{1/2}T_0^{1/2}} = O(1). \tag{3.42}$$

Equation (3.41) gives the approximate expression for the minimum radius, which requires that ϵ is small $(3.42)_1$ and that b, γ, and χ all be $O(1)$ as given in $(3.42)_{2-4}$.

4. Comparison with numerics. In previous work [16], a finite volume numerical framework was developed to solve the nonlinear conservation laws with the moving boundaries. Using this numerical framework, we run simulations on the asymptotic problem formulated in this paper. Our validation is done in multiple stages: we examine the profiles of the pulses during their formation both numerically and asymptotically by comparing the profiles of the resultant variables; then, we study the growths of the amplitudes of the pulses as they move radially inward as predicted by the asymptotics and numerics; we next proceed to study the existence of the residual velocity field with the numerics and the growth of the inner wall velocity with inner wall position; we observe that the velocity at the inner wall is qualitatively consistent with the numerical results; and finally, we compute the minimal radius in the asymptotic and numerical workings for various values of b, γ, χ, and ϵ.

We remark that the asymptotic problem we have considered is primarily concerned with a single direction of information propagation: the pulse travels toward the plasma

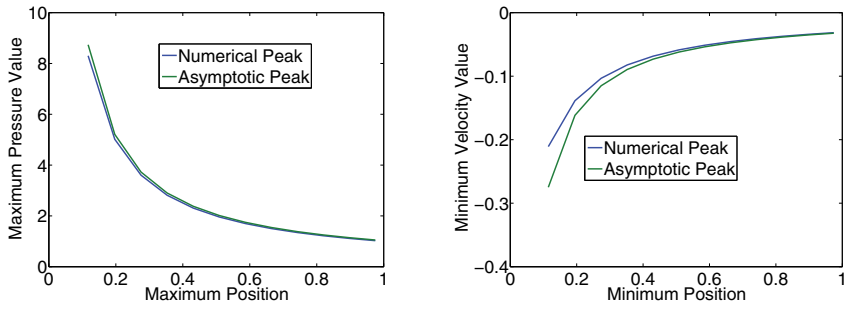

FIG. 5. *Numerical and asymptotic descriptions of the growth in peak values for the minimum value of velocity and peak value of pressure. Based on a best fit, the numerically observed scalings are* $1/r^{0.99}$ *and* $1/r^{0.90}$ *for the left and right plots, respectively. Parameters:* $b = \chi = \gamma = 1$, $\epsilon = 0.001$.

wall, it is reflected, and then everything else governing the plasma wall takes place locally near the wall and there is no influence from leftgoing waves. We need to exercise caution with this numerically by removing reflections that occur at the outer wall. This allows for better agreement between the asymptotics and numerics but we make two remarks. We first note that if these reflections are not removed, then a reflection occurs at the outer wall and disturbances return to hit the plasma again, which drastically reduces the compression. Such effects are noticeable for $\epsilon \lesssim 0.0025$. The second point to make is that even in attempting to remove the reflections at the outer wall, there is likely still a small numerical error that remains.

4.1. Pulse formation. We consider two parameter regimes here. One is for the parameter set of interest, and the other is for a much smaller ϵ with other dimensionless parameters set to unity. We fix an end time $t = \epsilon/2$ and plot the profiles of v and ρ as computed numerically, and with two different levels of asymptotic accuracy. From the plots, we are able to verify that the successive terms of the asymptotic expansion yield higher accuracies and that the asymptotics and numerics are in good agreement. See Figure 3.

4.2. Focusing. Here, we consider the asymptotically predicted growth rates for the peak amplitudes of the velocity and pressure. From the asymptotic predictions, both of these amplitudes should grow inversely with the position of these peaks. This validation is rather delicate: these growths should be upheld in the limit $\epsilon \downarrow 0$; however, there are difficulties in getting the numerics to give highly accurate results on regions where $r \ll 1$. What we choose to do is pick a very small value of ϵ, 0.001, and consider the growth of the amplitudes on the region $r > 0.1 \approx O(\sqrt{\epsilon})$. We plot the predictions as given by a perfect growth of $1/r$ based on the initial peak pressure and minimum velocity, and the numerical results for the peak amplitude versus position for this ϵ value. The plots are given in Figure 5 and we observe strong consistency.

4.3. Residual velocity field. Our prediction of a steady velocity field resulting from the disturbances interacting with the plasma was based primarily on intuition, as we did not formally find the solution for v_1 and ρ_2 for general $\hat{t}$; we simply showed that the potential approaches a constant value along the boundary. Numerically, however, we can validate the scaling. After a long time with respect to the $\hat{t}$ time scale so that v_0 has had its full effect, we plot the profile of the velocity versus the

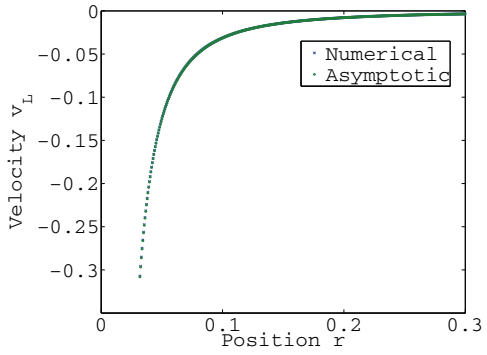

FIG. 6. *A plot of the numerical and asymptotic velocity profile after much of the pulses have reflected off the inner wall. The two are nearly indistinguishable. Parameters:* $b = \chi = \gamma = 1$, $\epsilon = 0.0025$, $t = 0.0784$.

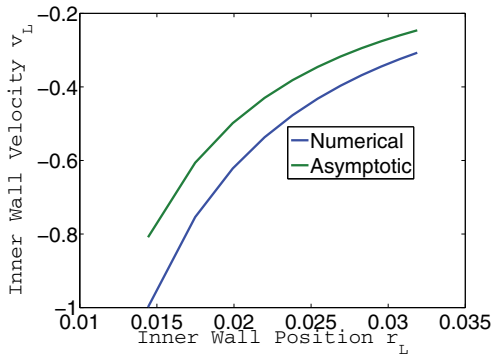

FIG. 7. *A plot of the numerical and asymptotic velocity profile for how the inner wall velocity implicitly depends on the inner wall position. Parameters:* $b = \chi = \gamma = 1$, $\epsilon = 0.0025$, t *ranging from* 0.0784 *to* 0.11.

radial position. As the inner wall moves inward, in its wake there is a velocity profile that scales like $1/r_L^2$. See Figure 6.

4.4. Outer region describing inner wall velocity. This validation is rather delicate as there are a number of sources of error. First, the inner wall position at which the boundary condition of (3.37) is better approximated by $\sigma = \chi - \sqrt{\epsilon}\frac{2\sqrt{\pi}}{b\chi}$ as per (3.24) but to leading order we have taken as $\sigma = \chi$. In the case considered in Figure 7, this already amounts to an error of 17% in estimating the boundary condition which will lead to an error in the constants obtained. We additionally know that $v \sim \sqrt{\epsilon}v_1 + \epsilon v_2$ so that there is an $O(\epsilon)$ error term in the radial position that is accrued over a time scale of $O(1)$. Throwing these effects together makes it very hard to get a clean fit between numerical and asymptotic results. In finding the slope of the $\log v_L$ versus $\log r_L$ plot, a least squares fit shows the numerical scaling is $v_L \propto 1/r_L^{1.49}$, which is completely consistent with the asymptotic scaling.

4.5. Qualitative agreement of inner wall velocity. The asymptotics predict a series of phenomena at the inner wall: first, the wall is stationary until the pressure pulse reaches it, whereupon it takes on a Gaussian shape then decreases in speed;

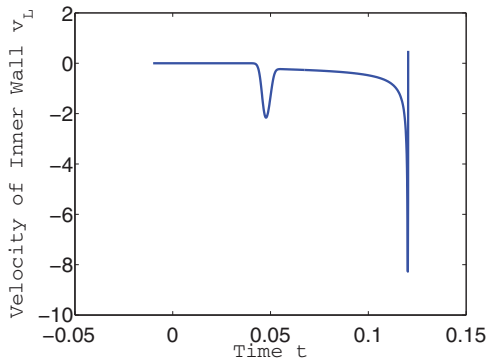

FIG. 8. *A numerical validation that the asymptotics have qualitatively captured the behavior of the inner wall. Parameters:* $b = \chi = \gamma = 1$, $\epsilon = 0.0025$.

TABLE 5

Asymptotic and numerical predictions of minimum radius of plasma for different values of ϵ *with* $b = 1.05, \chi = 0.937$, *and* $\gamma = \pi$. *Based on a least squares linear regression in a log-log plot of the difference versus* ϵ, *the convergence rate appears to be* $O(\epsilon^{2.3}) = o(\epsilon)$. *The convergence rate is excellent likely due to either small coefficients in the* $o(\epsilon)$ *asymptotic series terms or fortuitous cancellations of higher order asymptotic error terms.*

ϵ	r^*_{asy}	r^*_{num}	Error
0.02	0.02000	0.01155	0.00845
0.01	0.01000	0.00600	0.00400
0.005	0.00500	0.00444	0.00056
0.0025	0.00250	0.00242	0.00008

second, a smaller asymptotic term describing the wall velocity remains for some time (as the velocity acquires the residual profile); third, the wall rapidly speeds up; and finally, the wall is stopped abruptly on a small spatial scale when the plasma pressure finally takes over. We observe all these phenomena in Figure 8.

4.6. Predictions for plasma compression. In this section, we verify that the fundamental asymptotic predictions are consistent with the numerics. Table 5 presents the results. We remark that verifying the asymptotic limit is not trivial. As $\epsilon \downarrow 0$, the numerics, for modest discretizations, lose accuracy due to the very small radial positions under consideration. As a result, we cannot not take ϵ too small. We also have to ensure that quantities such as $b^4\chi^3\gamma/\pi$, etc., remained roughly $O(1)$ for these values of ϵ. Picking ϵ too large also leads to problems: for one, the higher order terms may dominate over the desired $r^* = O(\epsilon)$ behavior. Another issue is that if ϵ is not small enough, the apparently negligible displacement of the inner wall given by (3.24) could be larger than the initial inner radius of $\chi\sqrt{\epsilon}$. In Table 5, we compute the minimum radius asymptotically and numerically. We verify that the difference in the minimum radius between the asymptotic and exact (numerical) predictions is $o(\epsilon)$ when b, χ, and γ are fixed. We choose $b = 1.05, \chi = 0.937, \gamma = \pi$ so that the minimum radius should be 0.99994ϵ.

4.6.1. Comments on the model parameter regime. We anticipate as $b^4\chi^3\gamma/\pi$ moves farther from unity, along with other order one coefficients such as $\frac{\sqrt{2\pi}}{b^2\chi}$ in (3.26), the agreement between the asymptotic estimate and the numerical predictions of the minimum radius will weaken. With $b = 0.8, \chi = 1.19, \gamma = 3.52$, and $\epsilon = 0.01$,

then $b^4\chi^3\gamma/\pi = 0.77 \approx 1$ and the asymptotic and numerical predictions are 0.0077 and 0.0088, respectively: just a 13% relative error. With respect to the parameters of Table 3, $b^4\chi^3\gamma/\pi = 0.18 \not\approx 1$, where $b = 0.8$ has been replaced by $b = 0.557$, we have the respective asymptotic and numerical predictions as 0.00229 and 0.00649. The two predictions are of the same scale but are not quantitatively consistent. Despite the discrepancy, there is qualitative consistency between the numerical and asymptotic modeling. In previous work [16] where the model was very similar, the data show that perturbations to the inner radius had the greatest impact upon the compression. This was followed by a tie between maximum external pressure and maximum outer radius, and then pulse time scale, sound speed, and initial plasma pressure. This is reasonably consistent with (3.41), where based on the respective powers of the parameters, the relative sensitivity of the minimal radius with respect to the parameters (i.e., the percentage by which the minimal radius would change for a percent change in the parameter), from most to least sensitive follows the ordering of initial plasma radius; sound speed, initial outer radius, and maximum impulse pressure (three-way tie); pulse time scale; and initial plasma pressure. The proper positive/negative correlations are also consistent, i.e., when the asymptotics show an increase in a parameter decreases the radius, so do the numerics.

With the results of the asymptotics, we can make a few application-relevant statements. Based on $(2.14)_2$, (3.7), and (3.27), we note that only a small fraction of the energy input actually goes toward compressing the plasma. Indeed if we compute the energy input by

$$\int_{-\infty}^{\infty} \underbrace{-4\pi r_R(t)^2 p_R(t)}_{\text{force}} \underbrace{v_R(t)\mathrm{d}t}_{\text{displacement}} \sim \frac{4\pi\epsilon^{3/2}}{b}\int_{-\infty}^{\infty} e^{-2\tau^2}\mathrm{d}\tau = \frac{\sqrt{8\pi^3}}{b}\epsilon^{3/2},$$

the leading order energy is $O(\epsilon^{3/2})$ but only $O(\epsilon^{5/2})$ ultimately goes toward compression. A lot of energy is lost in reflection. In our modeling, we neglected the gas pressure of the plasma, which would also work to oppose the compression of the plasma; the degree the plasma is compressed is likely less than what we predict asymptotically, i.e., in a model with the gas pressure, r^* would be larger than our value given in (3.29) at leading order [15]. Also, based on the previous work mentioned in the previous paragraph, we can see that a smaller minimum radius does not necessary yield more promising fusion conditions (based on the Lawson triple product criterion [13]); the time over which the plasma is compressed is another vital element. While our work here predicts the minimum radius, this is only one of many complex components required for the success of magnetized target fusion.

5. Conclusions and future work. In this paper, an analytic result for the minimal radius of a plasma has been obtained in the limit of a very fast impulse time scale. Although the model is highly simplified, we can describe qualitatively the effects of key design parameters in the magnetized target fusion model in question. Equation (3.41) is qualitatively accurate, given the stipulations outlined in $(3.42)_{1-4}$, and it provides a good ballpark quantitative estimate for the minimum radius. The key parameters that are within control are likely $P_{\max}$, $R_{\text{outer},0}$, and T_0. In this case, within the limitations of the physical model, the plasma is compressed to a smaller and smaller radius as the piston pressure, initial outer radius, and pulse time scale all increase. If the medium through which the pressure pulses travel could be modified, then decreasing either its sound speed or density (or both) would be ideal while sustaining the piston pressure. Also, if the initial plasma pressure or size could be decreased, a greater compression can take place.

Although this problem contained nontrivial obstacles, including nonlinear conservation laws and moving boundaries, through appropriate scaling arguments and suitable solution techniques and estimates, an analytic result that agrees well with numerical simulations has been obtained in the limit where $\epsilon \downarrow 0$. Building upon this asymptotic framework, many new and important studies could potentially be done to enhance the physical accuracy and predictive power of the modeling, including adding detailed plasma physics, adding in the gas pressure and allowing for energy losses; considering the plasma and lead-lithium interaction more carefully; incorporating a more sophisticated equation of state for the lead-lithium; or even studying the effects of localized angular perturbations in the system given that perfect spherical symmetry is not physically realistic.

Acknowledgments. A huge thanks to Brian Wetton and Michael Ward of my advisory committee for their insights in this work and to Nilima Nigam and my officemates for their encouragement. Thank you to George Bluman for a relevant discussion on symmetry. Thanks to Sandra Barsky and Aaron Froese of General Fusion for helpful discussions. Thanks to the reviewers for their helpful feedback.

REFERENCES

[1] L. Artsimovich, *Controlled Thermonuclear Reactions*, Gordon and Breach Science Publishers, New York, 1964.
[2] C. Brennen, *Cavitation and Bubble Dynamics*, Oxford University Press, Oxford, UK, 1995.
[3] C. A. Coulson and A. Jeffrey, *Waves: A Mathematical Approach to the Common Types of Wave Motion*, Longman, New York, 1977.
[4] M. J. Edwards, P. K. Patel, J. D. Lindl, L. J. Atherton, S. H. Glenzer, S. W. Haan, J. D. Kilkenny, O. L. Landen, E. I. Moses, A. Nikroo, R. Petrasso, C. Sangster, P. T. Springer, S. Batha, R. Benedetti, L. Bernstein, R. Betti, D. L. Bleuel, T. R. Boehly, D. K. Bradley, J. A. Caggiano, D. A. Callahan, P. M. Celliers, C. J. Cerjan, K. C. Chen, D. S. Clark, G. W. Collins, E. L. Dewald, L. Divol, S. Dixit, T. Doeppner, D. H. Edgell, J. E. Fair, M. Farrell, R. J. Fortner, J. Frenje, M. G. Gatu Johnson, E. Giraldez, V. YU. Glebov, G. Grim, B. A. Hammel, A. V. Hamza, D. R. Harding, S. P. Hatchett, N. Hein, H. W. Herrmann, D. Hicks, D. E. Hinkel, M. Hoppe, W. W. Hsing, N. Izumi, B. Jacoby, O. S. Jones, D. Kalantar, R. Kauffman, J. L. Kline, J. P. Knauer, J. A. Koch, B. J. Kozioziemski, G. Kyrala, K. N. Lafortune, S. Le Pape, R. J. Leeper, R. Lerche, T. Ma, B. J. Macgowan, A. J. Mackinnon, A. Macphee, E. R. Mapoles, M. M. Marinak, M. Mauldin, P. W. McKenty, M. Meezan, P. A. Michel, J. Milovich, J. D. Moody, M. Moran, D. H. Munro, C. L. Olson, K. Opachich, A. E. Pak, T. Parham, H.-S. Park, J. E. Ralph, S. P. Regan, B. Remington, H. Rinderknecht, H. F. Robey, M. Rosen, S. Ross, J. D. Salmonson, J. Sater, D. H. Schneider, F. H. Seguin, S. M. Sepke, D. A. Shaughnessy, V. A. Smalyuk, B. K. Spears, C. Stoeckl, W. Stoeffl, L. Suter, C. A. Thomas, R. Tommasini, R. P. Town, S. V. Weber, P. J. Wegner, K. Widman, M. Wilke, D. C. Wilson, C. B. Yeamans, and A. Zylstra, *Progress towards ignition on the National Ignition Facility*, Phys. Plasmas, 20 (2013), 070501.
[5] E. Zaudere, *Partial Differential Equations of Applied Mathematics*, Wiley-Interscience Ser., Wiley, Hoboken, NJ, 1989.
[6] T. Faber, *Fluid Dynamics for Physicists*, Cambridge University Press, Cambridge, UK, 1995.
[7] E. Herbert, S. Balibar, and F. Caupin, *Cavitation pressure in water*, Phys. Rev. E, 74 (2006), 041603.
[8] E. Hinch, *Perturbation Methods*, Cambridge University Press, Cambridge, UK, 1991.
[9] V. Kedrinskii, *Hydrodynamics of Explosion: Experiment and Models*, Springer, Berlin, 2005.
[10] M. Laberge, *An acoustically driven magnetized target fusion reactor*, J. Fusion Energy, 27 (2007), pp. 65–68.
[11] M. Laberge, *Experimental results for an acoustic driver for MTF*, J. Fusion Energy, 28 (2009), pp. 179–182.
[12] L. D. Landau and E. M. Lifschitz, *Fluid Mechanics*, Pergamon Press, Elmsford, NY, 1959.
[13] J. Lawson, *Some criteria for a power producing thermonuclear reactor*, in Proceedings of the Physics Society, Section B, 1957, p. 70.

[14] D. K. Mansfield, K. W. Hill, J. D. Strachan, M. G. Bell, S. D. Scott, R. Budny, E. S. Marmar, J. A. Snipes, J. L. Terry, S. Batha, R. E. Bell, M. Bitter, C. E. Bush, Z. Chang, D. S. Darrow, D. Ernst, E. Fredrickson, B. Grek, H. W. Herrmann, A. Janos, D. L. Jassby, F. C. Jobes, D. W. Johnson, L. C. Johnson, F. M. Levinton, D. R. Mikkelsen, D. Mueller, D. K. Owens, H. Park, A. T. Ramsey, A. L. Roquemore, C. H. Skinner, T. Stevenson, B. C. Stratton, E. Synakowski, G. Taylor, A. Von Halle, S. Von Goeler, K. L. Wong, and S. J. Zweben, *Enhancement of Tokamak fusion test reactor performance by lithium conditioning*, Phys. Plasmas, 3 (1996), pp. 1892–1897.

[15] M. Lindstrom, *Investigation into the Feasibility and Operation of a Magnetized Target Fusion Reactor: Insights from Mathematical Modelling*, Ph.D. dissertation, University of British Columbia, 2015.

[16] M. Lindstrom, S. Barsky, and B. Wetton, *Investigation into fusion feasibility of a magnetized target fusion reactor: A preliminary numerical framework*, J. Fusion Energy, 34 (2014), pp. 76–83.

[17] L. Rayleigh, *On the pressure developed by a liquid during the collapse of a spherical cavity*, Philo. Mag. Ser. 6, 34 (1917), pp. 94–98.

[18] J. Ockendon, S. Howison, A. Lacey, and A. Movchan, *Applied Partial Differential Equations*, Oxford University Press, New York, 2003.

[19] S. D. Rothman, J.-P. David, J. Maw, C. M. Robinson, K. Parker, and J. Palmer, *Measurement of the principal isentropes of lead and lead-antimony alloy to ∼400 kbar by quasi-isentropic compression*, J. Phys. D, 38 (2005), pp. 733–740.

[20] G. B. Whitham, *Linear and Nonlinear Waves*, Wiley-Interscience Ser., Wiley, Hoboken, NJ, 1974.

[21] S. Woodruff, A. Macnab, and N. Mattor, *Adiabatic compression of a doublet field reversed configuration (FRC)*, J. Fusion Energy, 27 (2008), pp. 128–133.